

RSC Advances



This is an *Accepted Manuscript*, which has been through the Royal Society of Chemistry peer review process and has been accepted for publication.

Accepted Manuscripts are published online shortly after acceptance, before technical editing, formatting and proof reading. Using this free service, authors can make their results available to the community, in citable form, before we publish the edited article. This *Accepted Manuscript* will be replaced by the edited, formatted and paginated article as soon as this is available.

You can find more information about *Accepted Manuscripts* in the [Information for Authors](#).

Please note that technical editing may introduce minor changes to the text and/or graphics, which may alter content. The journal's standard [Terms & Conditions](#) and the [Ethical guidelines](#) still apply. In no event shall the Royal Society of Chemistry be held responsible for any errors or omissions in this *Accepted Manuscript* or any consequences arising from the use of any information it contains.

Water steam effect during the high CO₂ chemisorption in lithium cuprate (Li₂CuO₂) at moderate temperatures: experimental and theoretical evidences

Hugo A. Lara-García,¹ Brenda Alcántar-Vázquez,¹ Yuhua Duan² and Heriberto Pfeiffer^{1,*}

¹*Instituto de Investigaciones en Materiales, Universidad Nacional Autónoma de México, Circuito Exterior s/n Cd. Universitaria, Del. Coyoacán, CP 04510, México DF, Mexico.*

²*National Energy Technology Laboratory, United States Department of Energy, 626 Cochrans Mill Road, Pittsburgh, Pennsylvania 15236, United States.*

*Corresponding author. Phone; +52 (55) 5622 46 27, Fax; +52 (55) 5616 1371, Email; pfeiffer@iim.unam.mx

Abstract. Li₂CuO₂ was evaluated as CO₂ captor at moderate temperatures, using water vapor into the gas flow. Different water vapor sorption experiments were performed using N₂ or CO₂ as carrier gases. If N₂ was used as carrier gas, it was evidenced that Li₂CuO₂ is able to trap water physically and chemically, producing in the second case Li–OH superficial species. Moreover, when CO₂ was used as carrier gas, Li₂CuO₂ continued trapping water, as in the previous case, but in this case CO₂ was mainly trapped, forming Li₂CO₃ and CuO phases. Additionally, the microstructure change importantly when CO₂ and H₂O were chemically trapped in Li₂CuO₂. Li₂CO₃ and CuO seemed to segregate changing the morphology and the specific surface area. Li₂CuO₂ sample was able to capture up to 6.7 mmoles of CO₂ per gram of ceramic at 80 °C, a considerably high CO₂ amount. Furthermore, all these experiments were theoretically supported by different thermodynamic calculations. Experimental and theoretical results show that H₂O acts as a catalytic intermediate, diminishing the activation energy of the whole CO₂ chemisorption

process. Therefore, the presence of water vapor strongly favored the CO₂ chemisorption on Li₂CuO₂ at moderate temperatures (30-80 °C).

Keywords; CO₂ capture; Lithium cuprate; Thermal analysis, ab initio thermodynamics

1. Introduction

Nowadays, a main contributor to global warming and climate change problems is believed to be carbon dioxide (CO₂) produced due human activities, mainly from industrial gas streams.^{1,2} It is necessary to reduce the amounts of CO₂ gas produced. Numerous techniques (e.g., adsorption, chemisorption, cryogenic distillation, membrane separation) have been applied in order to reduce the amount of CO₂ emitted from large exhaust sources such as fossil fuel power plants, cement industries, iron and steel mills and other industry sectors which account for about 60 % of total CO₂ emissions.^{1,3}

Many studies have been focused on the development of solid CO₂ sorbents with high CO₂ sorption capacity and kinetics, good selectivity at low (30-200 °C), moderate (200-400 °C) or high temperature (>400 °C) and excellent regeneration ability.² In that way, some materials have been tested as CO₂ captors at low and moderate temperatures, such as carbon-based adsorbents, zeolites, hydrotalcites-like materials, metal-organic frameworks (MOFs), CaO-based sorbents and alkaline ceramics, among others.^{2,4-5} Among alkaline ceramics, lithium and sodium ceramics are the most studied at a wide temperature range (30-800 °C), for example zirconates, aluminates and silicates.⁶⁻³⁴

In addition, typical flow gas composition post-combustion contain approximately 65-75% N₂, 7-15% CO₂, 2-12% O₂, 5-15% H₂O, and smaller concentrations of other polluting species.³ Since water vapor is present in the flue gas post-combustion some works have been performed to understand the capture of CO₂ in different CO₂-H₂O compositions.

Particularly, among alkaline and earth alkaline ceramics, there are a few papers showing the effects of water vapor during de CO₂ absorption at low temperatures (30-80 °C).³⁴⁻⁴⁰ Most of these works mention that water vapor improve the CO₂ chemisorption due to the superficial hydroxylation processes. For example, it was recently published that CO₂ capture in Li₄SiO₄ is improved under the water vapor presence because the presence of steam enhances Li¹⁺ diffusion and reactivity between Li₄SiO₄ and CO₂.⁴⁰

On the other hand, lithium cuprate (Li₂CuO₂) presents interesting electronic and magnetic properties, so it has been used for different electrical applications such as cathodes for lithium-ion batteries and as a superconductor material, owing to the excellent lithium diffusion.⁴¹⁻⁴⁴ Some of these diffusion properties have been attributed to the Li₂CuO₂ layered crystalline structure, where the lithium atoms are located between the layers (Figure 1).⁴⁵ The Li₂CuO₂ presents an orthorhombic phase with the following unit cell parameters: a=3.655 Å, b=2.860 Å, c=9.377 Å and Z = 2.

Recently, it has been reported that the Li₂CuO₂ is able to trap CO₂ in a wide range of temperatures (120-650 °C).⁴⁶⁻⁴⁹ These papers show that Li₂CuO₂ is able to chemisorb CO₂, where the maximum theoretical CO₂ chemisorption capacity is 9.11 mmoles of CO₂ per gram of Li₂CuO₂ (0.401 g_{CO₂}/g_{ceramic}). These reports show that Li₂CuO₂ begins to react with CO₂ at around 120 °C in dry conditions. Thus, the presence of water vapor may improve the CO₂ chemisorption at low temperatures in this lithium ceramic. Therefore, the aim of the work reported here was to study the CO₂-H₂O capture process in Li₂CuO₂ at a low temperature range (30-80 °C).

2. Experimental section

Lithium cuprate (Li₂CuO₂) was synthesized by solid-state method. Initially, lithium

oxide (Li_2O , Aldrich) and copper oxide (CuO , Across Organics) were mixed mechanically, in order to get a good homogeneity of the reagents. The mixtures were prepared using a lithium excess of 10 wt%, based on the stoichiometric lithium content on Li_2CuO_2 , as lithium tends to sublime during high thermal treatments. Then, the powders were calcined at 800 °C for 6 h in air.

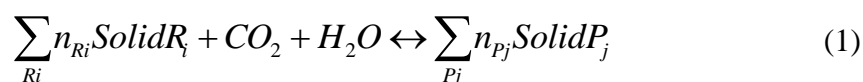
A diffractometer (Siemens D-5000) coupled to an X-ray tube was used to identify the phases obtained. The phase was identified using the Joint Committee Powder Diffraction Standards (JCPDS) files. The microstructural characteristics of the Li_2CuO_2 sample was determined via N_2 adsorption-desorption and scanning electron microscopy (SEM). N_2 adsorption (Bel-Japan Minisorp II) was used to determine the sample surface area using the BET model. Then, the sample morphology was analyzed by SEM, which was performed on a JEOL JMS-7600F.

The CO_2 - H_2O sorption process was evaluated dynamic and isothermally in a humidity-controlled thermobalance (TA Instruments, model Q5000SA) at different temperatures and relative humidity (RH). The experiments were performed using distilled water and two different flow gases: nitrogen (N_2 , Praxair grade 4.8) or carbon dioxide (CO_2 , Praxair grade 3.0). The total flow gas used in all the experiments was 100 mL/min and the RH percentages were controlled automatically by the Q5000SA equipment. Dynamic water vapor sorption/desorption experiments were generated at different temperatures (between 30 and 80 °C), varying the RH from 0 to 80 % (sorption) and then from 80 to 0 % (desorption) at a rate of 0.5 %/min, using 100 mL of N_2 or CO_2 as flow gas during the entire experiment. Additionally, different isothermal experiments were

performed at specific temperatures (20, 40, 60 and 80 °C) setting the RH at different values (20, 40, 60 and 80 %) for 180 min, using CO₂ as carrier gases.

Afterwards, the CO₂ isothermal products (~40mg) were characterized to identify and quantify the products. The samples were analyzed using XRD, infrared spectroscopy (FTIR), and thermogravimetric analysis (TGA). XRD characterization was performed as described above. For FTIR spectroscopy samples were analyzed in an Alpha-Platinum spectrometer from Bruker, using the ATR mode. The TG measurements were performed under a nitrogen atmosphere using a TA Instruments model Q500HR thermobalance from 30 to 930 °C at a rate of 5°C/min. Additionally, to elucidate if these products presented changes in their microstructural characteristics, the isothermal products were analyzed via N₂ adsorption-desorption and scanning electron microscopy (SEM) using the same methods described above.

Since the thermodynamic properties of the Li₂CuO₂ are not available in the literature, we performed the *ab initio* thermodynamics calculations on these CO₂ capture reactions by Li₂CuO₂ based on combining density functional theory (DFT) with lattice phonon dynamics. The detailed descriptions of the calculation method can be found in previous studies.⁵⁰⁻⁵² The CO₂ and/or H₂O capture reactions of Li₂CuO₂ can be expressed generically in the form (for convenient description, we normalized the reaction to 1 mole of CO₂ or H₂O):



where n_{R_i} , n_{P_j} are the reagents (R_i) and products (P_j) moles involved in the capture reactions. We treat the gas phase CO₂ or H₂O as an ideal gas. By assuming that the difference between the Gibbs free energy (ΔG°) of the solid phases of reactants (R_i) and

products (P_j) can be approximated by the difference in their total energies (ΔE_{DFT}), obtained directly from DFT calculations, and the vibrational free energy of the phonons and by ignoring the PV contribution terms for solids, the variation of the chemical potential ($\Delta\mu$) for reaction with temperature and pressure can be written as:

$$\Delta G(T, P) = \Delta G^0(T) - RT \ln \frac{P_{gas}}{P_0} \quad (2)$$

where,

$$\Delta G^0(T) \approx \Delta E_{DFT} + \Delta E_{ZP} + \Delta F_{PH}(T) - G_{gas}^0(T) \quad (3)$$

Here, ΔE_{DFT} is the DFT energy difference between the reactants and products of the reaction ΔE_{ZP} is the zero point energy difference between the reactants and products and can be obtained directly from phonon calculations. ΔF_{PH} is the phonon free energy change excluding zero-point energy (which is already counted into the ΔE_{ZP} term) between the solids of products and reactants. P_{gas} is the partial pressure of CO₂ or H₂O in the gas phase and P_0 is the standard state reference pressure taken to be 1 bar. The heat of reaction ($\Delta H^{cal}(T)$) can be evaluated through the following equation:

$$\Delta H^{cal}(T) = \Delta G^o(T) + T[\Delta S_{PH}(T) - S_{CO_2}(T)] \quad (4)$$

where, $\Delta S_{PH}(T)$ is the difference of entropies between product solids and reactant solids. The free energy of CO₂ or H₂O (G_{gas}^0) can be obtained from standard statistical mechanics,⁵¹⁻⁵³ and its entropy (S_{gas}) can be found in the empirical thermodynamic databases.⁵⁴ The DFT calculations with plane-wave basis sets and pseudopotential approximation were done to describe the structural, energetic and electronic properties of solids considered in this study. All calculations were performed using the Vienna *ab-initio* simulation package (VASP).^{55,56} In this study, the PAW pseudo-potentials and PW91 exchange-correlation

functional were used in all of the calculations. Plane wave basis sets were used with a kinetic energy cutoff of 520 eV and an augmentation charge cutoff of 605.4 eV. The k-point sampling grids of $m \times n \times l$, obtained using the Monkhorst-Pack method,⁵⁷ are used for these bulk calculations, where m , n , and l are determined with a spacing of about 0.028 Å⁻¹ along the reciprocal axes of their unit cells. In the phonon calculations, for each generated supercell, the displacements of 0.03 Å of non-equivalent atoms were generated. Then, for each supercell, the DFT calculations were performed again to obtain the force on each atom due to the displacements. These forces are carried back to PHONON package⁵⁸ to calculate the phonon dispersions and densities from which the partition function can be carried out and used to obtain free energies and entropies as shown in Equations.3 and 4.

3. Results and discussion

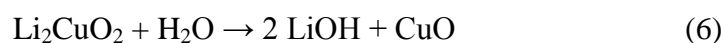
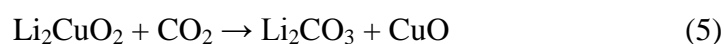
Figure 2 shows the XRD pattern of the Li₂CuO₂ synthesized by solid state reaction. The diffraction pattern fitted to the 00-084-1971 JCPDS file, and no other phases were detected. After the structural confirmation, the sample microstructure was analyzed by N₂ adsorption and SEM. The Li₂CuO₂ morphological characteristics are shown in the Figure 3. The size of the Li₂CuO₂ agglomerates is around 5-15 μm, but a closer analysis indicated that these agglomerates are formed by polyhedral particles of 0.5 μm in average. Additionally, the N₂ adsorption-desorption isotherm for this sample corresponded to a type II isotherm according to the IUPAC classification (data shown below)⁵⁹ and the isotherm did not presented hysteresis. Additionally, the surface area of the sample was estimated to be 0.2 m²/g using the BET model. This behavior corresponds to a nonporous, dense aggregate of particles, which is in good agreement with the synthesis method (solid-state reaction) and SEM observations.

Experimentally, $\text{Li}_2\text{CuO}_2\text{-N}_2\text{-H}_2\text{O}$ and $\text{Li}_2\text{CuO}_2\text{-CO}_2\text{-H}_2\text{O}$ systems were evaluated at different temperatures (30–80 °C). The $\text{Li}_2\text{CuO}_2\text{-N}_2\text{-H}_2\text{O}$ system was analyzed seeking for any possible reaction between lithium cuprate and water vapor. Figure 4 shows water vapor sorption-desorption isotherms. It is clearly evident that all of the sorption isotherms corresponded to type III according to the IUPAC classification.⁵⁹ Water sorption varied as a function of the temperature, and it was not completed or limited to the increasing relative humidity section ramp (0–80% RH) because during some part of the decreasing RH section ramp (80–0% RH), the samples continued gaining weight. This effect was highly evidenced in the isotherm performed at 80 °C. Therefore, as these curves are dynamic experiments the water sorption equilibrium has not been reached. Final weight increments into the $\text{N}_2\text{-H}_2\text{O}$ flow did not vary importantly. While the Li_2CuO_2 sample treated at 40 °C gained 10.3 wt %, the final weight increment at 80 °C was 15.5 wt %. However, the sorption process began at a much lower RH when temperature was increased. At 40 °C, the weight increased at around 38 % of RH, while the sorption process began with 14 % of RH at 80 °C. It must be mentioned that the weight decrement observed in the sample thermally treated at 80 °C during the desorption process between 35 and 14 wt% must be attributed to water evaporation. In previous works, the final weight increments observed during the $\text{N}_2\text{-H}_2\text{O}$ flow experiments has been attributed to a surface hydroxylation process, where different species are produced.³⁵⁻³⁹

Figure 5 shows the $\text{Li}_2\text{CuO}_2\text{-CO}_2\text{-H}_2\text{O}$ sorption-desorption curves. Again, the sorption curves were type III, as in the previous case, but the water desorption process and the final weight increments were noticeably different. In all these cases, the weight gain increased as a function of the temperature, from 4.9 to 30.2 wt % at 30 and 80 °C, respectively. It means that the final weight gained is twice larger in the $\text{CO}_2\text{-H}_2\text{O}$ system (at

80 °C) in comparison to the N₂-H₂O case. Therefore, the CO₂-H₂O system produces different reactions than N₂-H₂O, where hydration, hydroxylation, and carbonation processes must be performed.

Table 1 and Figures 6 and 7 show the calculated thermodynamic properties of CO₂ reactions with Li₂CuO₂ and LiOH (reactions 5 and 7), as well as the Li₂CuO₂ hydroxylation reaction (reaction 6), because lithium hydroxide seems to be the real responsible of the CO₂ capture under humidity conditions.



As shown in Figure 6A, the heat of reactions (ΔH) involved in these three reactions, obey the Hess's law, and all of them are exothermic reactions. For example at 27 °C, the Li₂CuO₂ carbonation reaction (reaction 5) has a ΔH value of -185 kJ/mol, whilst the Li₂CuO₂ hydroxylation and subsequent carbonation processes (reactions 6 and 7) have ΔH values equal to -86 and -98 kJ/mol, respectively. In other words, the total ΔH value of reactions 6 and 7 is -184 kJ/mol, the alike energy required in reaction 5. The same tendency is observed in the whole temperature range. On the other hand, and according the ΔG values (Figure 6B), the Li₂CuO₂ hydroxylation and LiOH carbonation reactions (reactions 6 and 7) are less stable than Li₂CuO₂ direct carbonation. Thus, ΔG values indicate that Li₂CuO₂-CO₂-H₂O reaction system is stabilized as Li₂CO₃ and CuO, where H₂O simply acts as a catalytic intermediate. In other words, these thermodynamic data confirm that water acts as intermediate specie in the Li₂CuO₂-CO₂-H₂O system diminishing the activation energy of the whole reaction process.

Moreover, Figure 7 shows T and P graphs describing where the chemical potential is equal to zero for the reactions 5-7, where $\Delta G = 0$. Around $\text{Li}_2\text{CuO}_2\text{-CO}_2$ and LiOH-CO_2 reaction lines are determined the chemisorption and desorption regions with optimal conditions because of the minimum energy costs at the respective temperature and pressure conditions. Additionally, in the $\text{Li}_2\text{CuO}_2\text{-H}_2\text{O}$ reaction curve, the hydroxylation and dehydroxylation regions are determined. All these reactions are thermodynamically favorable over a certain range of temperatures and P_{CO_2} or $P_{\text{H}_2\text{O}}$, which means that under such conditions CO_2 and H_2O are thermodynamically favored to be reacted with Li_2CuO_2 or LiOH . However, it is evident that the CO_2 capture is more favored than the dehydroxylation process under the experimental conditions of temperature and CO_2 pressure. Based in the theoretical and experimental results, the most feasible reaction mechanism is the Li_2CuO_2 hydroxylation process subsequently followed by the LiOH carbonation process. Nevertheless, at standard pressures the CO_2 chemisorption in both materials (Li_2CuO_2 or LiOH) is favored over the Li_2CuO_2 hydroxylation process.

To further understand and analyze the influence of water during the CO_2 capture in Li_2CuO_2 , different kinetic experiments are presented in Figure 8, and these isothermal products were re-characterized to determine and quantify the species produced. Isothermal experiments were performed between 40 and 80 °C at different RH (20, 40, 60, and 80%). Weight increment rates and amounts increased as a function of the RH, as it could be expected. At 40 °C the samples treated with 20 and 40% of RH only increased their weights in 0.2 and 1.2 wt % after 3 h, respectively. When the RH was increased to 60 and 80 %, the final weights were 9.2 and 20.5 wt %, respectively. Similar trends were observed at 60 and 80 °C. Nevertheless, the final weight increments increased as a function of temperature and

RH. It can be well represented if the isotherms with 80 % of RH are compared at different temperatures. The final weights in these cases were 20.5, 24.1 and 37.6 wt% at 40, 60 and 80 °C, respectively. It must be mentioned that after the experimental times none of these isothermal conditions reached the equilibrium. So the CO₂ capture must continue at longer times.

To confirm the CO₂ chemical capture and to quantify the CO₂ through the Li₂CO₃ formation under the different thermal and RH conditions, all the isothermal products were characterized using XRD and TGA, through decomposition thermograms. Figure 9 shows the XRD pattern of one specific isothermal product as an example (80 °C and 80 % of RH), where the CO₂ chemical capture was confirmed by the Li₂CO₃ and CuO formation (see reactions 5-7). In this XRD pattern LiOH was not identified. This result strongly suggest that most of the LiOH reacted with CO₂, producing Li₂CO₃. In fact, this qualitative evidence was corroborated by the TG decomposition analysis described now. Figure 10 shows the TG and DTG decomposition curves of isothermal products treated at 80 °C with different RH. These thermograms show three different decomposition processes. Initially, between room temperature and 120 °C, the samples lost small quantities of weight (around 1 and 2.5 wt%), which could be attributed to dehydration processes. The second weight decrement was observed between 350 and 470 °C, and it can be attributed to the dehydroxylation process. In fact, the samples treated at lower RH presented lower dehydroxylations than those observed at high HR. Additionally, the DTG dehydroxylation peaks were shifted to higher temperatures as a function of the RH, which may be related to the carbonation process. If the Li₂CO₃ shell amounts are higher, the dehydroxylation may become slower due to diffusion processes. In fact, this assumption is in good agreement with the decarbonation process, which was produced at $T \geq 600$ °C. The decarbonation

process was produced in two steps between 610 and 760 °C and between 760 and 925 °C. These two processes can be described as superficial and bulk decarbonation processes. Based in these results the amounts of CO₂, trapped as Li₂CO₃ (weight lost at T 600 ≥ °C), were quantified and plotted in Figure 11. From these curves it is obvious that when the RH increased from 20 to 80%, the CO₂ chemisorbed increased, independently of the temperature, although the CO₂ chemisorptions at 80 °C presented the best results, where the maximum weight increment (29.5 wt%) was obtained at 80 °C and 80 % of RH. This weight increment corresponds to a 72.2 % of the total efficiency, although the equilibrium was not reached. So the CO₂ chemisorption may be increased as a function of time. The efficiency obtained after 3 hours corresponds to 6.6 mmoles of CO₂ per gram of Li₂CuO₂. In addition, it could be mentioned that if Li₂CuO₂ reacted totally with CO₂, the maximum theoretical CO₂ capture value would correspond to 9.13 mmoles/g (see reaction 5).

Li₂CuO₂ and other alkaline ceramics have shown good CO₂ capture properties at moderate temperatures in the presence of water steam; in comparison to dry conditions.³⁵⁻⁴⁰ The explanation given for this effect has been associated to the ceramic hydroxylation process, which promotes the CO₂ reactivity. On the other hand, different microstructural characteristics may have been modified during the CO₂ chemisorption process. So, the Li₂CuO₂-CO₂-H₂O isothermal products were analyzed by SEM and N₂ adsorption. Figure 12 show some secondary and backscattered electron images (BSEI) of the Li₂CuO₂-CO₂-H₂O isothermal products treated at 80 °C with 80 % of RH. The morphology of the sample changed importantly in comparison to the Li₂CuO₂ initial appearance (see Figure 3). The particles seem to be still agglomerated but the polyhedral particles decreased in size importantly, from 15 μm to 200 nm. Additionally, BSEI analysis evidenced the presence of

two different phases by the particle contrasts observed in the corresponding image. These two phases must correspond to Li_2CO_3 and CuO , because they are the main Li_2CuO_2 carbonation products (excluding the possible hydroxide formation). Thus, the contrast differences arise from the differences in mean atomic number (\bar{Z}) of Li_2CO_3 and CuO , 6 and 18.5, respectively. Therefore, the backscattered electron coefficient (η)⁶⁰ of these phases increases from 0.064 to 0.212 for Li_2CO_3 (dark phase) and CuO (light phase), respectively. From this backscattered electron image, it can be observed that CuO nanoparticles (≤ 200 nm) seem to be dispersed over the Li_2CO_3 phase. Finally, the N_2 adsorption-desorption isotherm of the pristine Li_2CuO_2 sample and the isothermal product treated at 80 °C and 80 % of RH are presented in the Figure 13. Both samples are isotherms type II, to the IUPAC classification,⁵⁹ but only the isothermal product presented hysteresis, H3 type. The presence of hysteresis and the large difference in the N_2 adsorbed volume clearly indicate high variations in the textural properties of these samples. Additionally, the surface areas of these samples were determined using the BET model. While the surface area of the pristine Li_2CuO_2 sample was 0.2 m^2/g , the isothermal product had a surface area of 11.3 m^2/g . The large difference observed between these samples may be associated Li_2CO_3 - CuO external shell, which resulted to have porous and the formation of CuO nanoparticles, determined by SEM. Similar results have been published for other alkaline ceramics during the CO_2 capture.⁶⁻³⁴ Nevertheless, these textural modifications have been observed at much higher temperatures (450-550 °C) during the CO_2 capture process under dry conditions. In any case, the presence of porosity and/or the nanoparticles formation allows CO_2 or CO_2 - H_2O diffusion, favoring the CO_2 chemisorption without the necessity of intercrystalline processes. All these results are in good agreement with the SEM and isothermal results.

All these results clearly show that CO₂ chemisorption in Li₂CuO₂ is importantly improved by the presence of water vapor in moderate temperatures (30–80 °C), in comparison to the dry conditions, as Li₂CuO₂ only chemisorbs CO₂ at higher temperatures than 250 °C under dry conditions.^{46–49} If these amounts of CO₂ trapped are compared with other materials, the results seem to be highly encouraging. For example, several materials including activated carbons, zeolites, hydrotalcites, and amines, are able to trap, physically or chemically, around 4–6 mmol/g in the same temperature range.^{4,5,61,62} In addition, other alkaline ceramics (Li₅AlO₄ and Na₂ZrO₃, among others) tested as CO₂ captors in similar thermal and humid conditions have shown similar properties.^{35–39} Nevertheless, the Li:Al molar ratio on Li₅AlO₄ is importantly higher (4:1) than those of Na₂ZrO₃ and Li₂CuO₂ (2:1). Hence, the high CO₂ chemisorption in Li₅AlO₄ at low temperatures may be attributed to the high lithium content, while in the Li₂CuO₂ case could be attributed to the high lithium accessibility presented due to its layered crystalline structure. In fact the Na₂ZrO₃ has the same alkaline:metal atomic molar ratio as well as the layered crystalline structure. Consequently, it seems that layered crystalline structures highly favor the CO₂ reactivity with Li₂CuO₂. Thus, this kind of ceramics may be considered as feasible materials for the CO₂ capture at moderate temperatures.

4. Conclusions

The Li₂CuO₂-CO₂-H₂O system was evaluated at moderate temperatures (30–80 °C). Li₂CuO₂ sample was prepared by solid-state reaction. Initial results, using N₂ as carrier gas, showed that Li₂CuO₂ traps water physically and chemically, where the water vapor adsorption and/or chemisorption depended on temperature and relative humidity. When CO₂ was used as carrier gas, important changes appeared in the results. Although Li₂CuO₂

mainly trapped CO₂ chemically, producing Li₂CO₃ and CuO. In fact, different isothermal analyses and the characterization of the isothermal products confirmed this statement. Li₂CuO₂ was able to chemisorb 6.7 mmoles of CO₂ per gram of ceramic.

Additionally, all previous results were corroborated based on the theoretical thermodynamic data for the Li₂CuO₂-CO₂, Li₂CuO₂-H₂O and LiOH-CO₂ reaction systems. ΔH and ΔG values clearly showed the different thermal stability of each reaction process at different temperature ranges, but lithium cuprate carbonation is the most plausible process at moderate temperatures. All the experimental and theoretical results showed that H₂O acts as catalytic intermediate specie, which must diminish the activation energy of the whole CO₂ chemisorption process. Thus, Li₂CuO₂ must be considered as a possible option for the CO₂ capture process at moderated or environmental temperatures.

Acknowledgements

This work was financially supported by the projects PAPIIT-UNAM (IN-102313) and SENER-CONACYT (150358). H. Lara-García thanks CONACYT for financial support. The authors thank to Adriana Tejeda and Omar Novelo for technical help.

References

1. J. D. Figueroa, T. Fout, S. Plasynski, H. McIlvried, R. D. Srivastava, *Int. J. Greenhouse Gas Control*, 2008, **2**, 9–20.
2. J. Wang, L. Huang, R. Yang, Z. Zhang, J. Wu, Y. Gao, Q. Wang, D. O'Hare, Z. Zhong, *Energy Environ. Sci.*, 2014, **7**, 3478-3518.
3. P. Wattanaphan, T. Sema, R. Idem, Z. Liang, P. Tontiwachwuthikul, *Int. J. Greenhouse Gas Control*, 2013, **19**, 340–349.

4. S. Choi, J. Drese, C. Jones, *Chem. Sus. Chem.*, 2009, **2**, 796–854.
5. S. D. Kenarsari, D. Yang, G. Jiang, S. Zhang, J. Wang, A. G. Russell, Q. Wei, M. Fan, *RSC Adv.*, 2013, **3**, 22739-22773.
6. Y. Duan, D. Luebke, H. Pennline, *Int. J. Clean Coal Energy*, 2012, **1**, 1-11.
7. P. V. Subha, B. N. Nair, P. Hareesh, A. P. Mohamed, T. Yamaguchi, K. G. K. Warriar, U. S. Hareesh, *J. Mater. Chem A*, 2014, **2**, 12792-12798.
8. J. Ida, J. Y. S. Lin, *Environ. Sci. Technol.* 2003, **37**, 1999–2004.
9. H. Pfeiffer, C. Vazquez, V. H. Lara, P. Bosch, *Chem. Mater.* 2007, **19**, 922–926.
10. A. Iwana, H. Stephensonb, W. Ketchiec, A. Lapkin, *Chem. Eng. J.* 2009, **146**, 249–258.
11. E. Ochoa-Fernández, M. Rønning, T. Grande, D. Chen, *Chem. Mater.* 2006, **18**, 1383–1385.
12. L. Martínez-dlCruz, H. Pfeiffer, *Ind. Eng. Chem. Res.* 2010, **49**, 9038–9042.
13. Q. Xiao, Y. Liu, Y. Zhong, W. Zhu, *J. Mater. Chem.*, 2011, **21**, 3838-3842.
14. I. Alcérreca-Corte, E. Fregoso-Israel, H. Pfeiffer, *J. Phys. Chem. C*, 2008, **112**, 6520–6525.
15. L. Martínez-dlCruz, H. Pfeiffer, *J. Phys. Chem. C*, 2012, **116**, 9675–9680.
16. B. Alcántar-Vázquez, C. Diaz, I. C. Romero-Ibarra, E. Lima, H. Pfeiffer, *J. Phys. Chem. C*, 2013, **117**, 16483–16491.
17. T. Zhao, E. Ochoa-Fernández, M. Ronning, D. Chen, *Chem. Mater.* 2007, **19**, 3294–3301.
18. L. Martínez-dlCruz, H. Pfeiffer, *J. Solid State Chem.* 2013, **204**, 298–304.
19. B. Alcántar-Vázquez, J. F. Gómez-García, G. Tavizon, I. A. Ibarra, C. Diaz, E. Lima, H. Pfeiffer, *J. Phys. Chem. C*, 2014, **118**, 26212–26218.

20. T. Ávalos-Rendón, J. Casa-Madrid, H. Pfeiffer, *J. Phys. Chem. A*, 2009, **113**, 6919–6923.
21. X. Jiao, H. Li, L. Li, F. Xiao, N. Zhao, W. Wei, *RSC Adv.*, 2014, **4**, 47012-47020.
22. V. Mejia-Trejo, E. Fregoso-Israel, H. Pfeiffer, *Chem. Mater.* 2008, **20**, 7171–7176.
23. C. Gauer, W. Heschel, *J. Mater. Sci.* 2006, **41**, 2405–2409.
24. R. Rodríguez-Mosqueda, H. Pfeiffer, *J. Phys. Chem. A*, 2010, **114**, 4535–4541.
25. M. Kato, K. Nakagawa, K. Essaki, Y. Maezawa, S. Takeda, R. Kogo, Y. Hagiwara, *Int. J. Appl. Ceram. Technol.* 2005, **2**, 467–475.
26. M. Kato, S. Yoshikawa, K. Nakagawa, *J. Mater. Sci. Lett.* 2002, **21**, 485–487.
27. S. Wang, C. An, Q. H. Zhang, *J. Mater. Chem. A*, 2013, **1**, 3540-3550.
28. T. Okumura, K. Enomoto, N. Togashi, K. Oh-Ishi, *J. Ceram. Soc. Jpn.* 2007, **115**, 491–497.
29. K. Essaki, K. Nakagawa, M. Kato, H. Uemoto, *J. Chem. Eng. Jpn.* 2004, **37**, 772–777.
30. K. Essaki, M. Kato, H. Uemoto, *J. Mater. Sci.* 2005, **18**, 5017–5019.
31. S. Y. Shan, Q. M. Jia, L. H. Jiang, Q. C. Li, Y. M. Wang, J. H. Peng, *Ceram. Int.* 2013, **39**, 5437–5441.
32. Z. Qi, H. Daying, L. Yang, Y. Qian, Z. Zibin, *AIChE J.* 2013, **59**, 901–911.
33. S. Kumar, S. K. Saxena, *Mater. Renew. Sustain. Ener.*, 2014, **3**:30.
34. J. Fagerlund, J. Highfield, R. Zevenhoven, *RSC Adv.*, 2012, **2**, 10380-10393.
35. L. Martinez-dlCruz, H. Pfeiffer, *J. Phys. Chem. C*, 2010, **114**, 9453-9458.
36. G. G. Santillan-Reyes, H. Pfeiffer, *Int. J. Greenhouse Gas Control*, 2011, **5**, 1624–1629.
37. J. Ortiz-Landeros, C. Gomez-Yañez, H. Pfeiffer, *J. Solid State Chem.* 2011, **184**, 2257–2262.

38. T. Ávalos-Rendon, H. Pfeiffer, *Energy & Fuels*, 2012, **26**, 3110–3114.
39. R. Rodríguez-Mosqueda, H. Pfeiffer, *J. Phys. Chem. C*, 2013, **117**, 13452–13461.
40. S. Zhang, Q. Zhang, H. Wang, Y. Ni, Z. Zhu, *Int. J. Hydrogen. Energ.* 2014, **39**, 17913–17920.
41. E. M. L. Chung, G. J. McIntyre, D. M. Paul, G. Balakrishnan, M. R. Lees, *Phys. Rev. B*, 2003, **68**, 144410.
42. A. S. Prakash, D. Larcher, M. Morcrette, M. S. Hegde, J.-B. Leriche, C. Masquelier, *Chem. Mater.* 2005, **17**, 4406-4415.
43. G. Vitins, E. A. Raekelboom, M. T. Weller, J. R. Owen, *J. Power Sources*, 2003, **119–121**, 938-942.
44. K. Nakamura, K. Kawai, K. Yamada, Y. Michihiro, T. Moriga, I. Nakabayashi, T. Kanashiro, *Solid State Ionics*, 2006, **177**, 2775-2778.
45. F. Sapina, J. Rodriguez-Carvajal, M. J. Sanchis, R. Ibanez, A. Beltran, D. Beltran, *Solid State Commun.* 1990, **74**, 779-784.
46. L. M. Palacios-Romero, H. Pfeiffer, *Chem. Lett.* 2008, **37**, 862-863.
47. L. M. Palacios-Romero, E. Lima, H. Pfeiffer, *J. Phys. Chem. A*, 2009, **113**, 193–198.
48. Y. Matsukura, T. Okumura, R. Kobayashi, K. Oh-ishi, *Chem. Lett.* 2010, **39**, 966-967.
49. K. Oh-ishi, Y. Matsukura, T. Okumura, Y. Matsunaga, R. Kobayashi, *J. Solid State Chem.* 2014, **211**, 162–169.
50. Y. Duan, H. Pfeiffer, B. Y. Li, I. C. Romero-Ibarra, D. C. Sorescu, D. R. Luebke, and J. W. Halley, *Phys. Chem. Chem. Phys.* 2013, **15**, 13538-13558.
51. Y. Duan, D. C. Sorescu, *Phys. Rev. B*, 2009, **79**, 014301.
52. Y. Duan, D. C. Sorescu, *J. Chem. Phys.* 2010, **133**, 074508.
53. B. Zhang, Y. Duan, J. K. Johnson, *J. Chem. Phys.* 2012, **136**, 064516.

54. M. W. J. Chase, NIST-JANAF Thermochemical Tables, 4th edition, *J. Phys. Chem. Ref. Data*, Monograph 1998, **9**, 1 1951.
55. G. Kresse, J. Hafner, *Phys. Rev. B*, 1993, **47**, 558-561.
56. G. Kresse, J. Furthmuller, *Comput. Mater. Sci.* 1996, **6**, 15-50.
57. H. J. Monkhorst, J. D. Pack, *Phys. Rev. B*, 1976, **13**, 5188 5192.
58. K. Parlinski, *Software PHONON*, Computing for Materials: Krakow, Poland, 2006.
59. S. Lowell, J. E. Shields, M. A. Thomas, *Particle Technology Series; Kluwer Academic Publishers*, London, 2004.
60. H. Pfeiffer, K. Knowles, *J. Eur. Ceram. Soc.* 2004, **24**, 2433–2443.
61. Q. Wang, J. Luo, Z. Zhong, A. Borgna, *Energy Environ. Sci.* 2011, **4**, 42-55.
62. D. A. Torres-Rodríguez, E. Lima, J. S. Valente, H. Pfeiffer, *J. Phys. Chem. A*, 2011, **115**, 12243–12250.
63. Y. Duan, B. Zhang, D. C. Sorescu, J. K. Johnson, *J. Solid State Chem.* 2011, **184**, 304-311.

Figure captions

Figure 1. Crystal structure of Li_2CuO_2 in space group Immm (No. 71). Red stands for oxygen, purple stands for lithium, and gray stands for copper.

Figure 2. X-ray diffraction pattern of the Li_2CuO_2 synthesized by solid state reaction.

Figure 3. Secondary electron images of the Li_2CuO_2 sample.

Figure 4. $\text{Li}_2\text{CuO}_2\text{-N}_2\text{-H}_2\text{O}$ sorption-desorption curves where different weight increments are shown as a function temperatures (40-80 °C).

Figure 5. $\text{Li}_2\text{CuO}_2\text{-CO}_2\text{-H}_2\text{O}$ sorption-desorption curves where different weight increments are shown as a function temperatures (40-80 °C).

Figure 6. The calculated thermodynamic data of different reactions of Li_2CuO_2 and LiOH capturing CO_2 *versus* temperatures, as well as the Li_2CuO_2 hydroxylation reaction: (A) heat of reaction (ΔH) and (B) free energy (ΔG).

Figure 7. The calculated vant' Hoff Plots of the relationships among the free energy (ΔG), temperature (T) and gas pressure (P in logarithmic scale). It has to be mentioned that only the $\Delta G=0$ curves are presented here. For $\text{Li}_2\text{CuO}_2 + \text{CO}_2 = \text{Li}_2\text{CO}_3 + \text{CuO}$, $P=P_{\text{CO}_2}/P_0$, where P_0 is the reference pressure set to 1 bar; For $2\text{LiOH} + \text{CO}_2 = \text{Li}_2\text{CO}_3 + \text{H}_2\text{O}$. For $\text{Li}_2\text{CuO}_2 + \text{H}_2\text{O} = 2\text{LiOH} + \text{CuO}$, $P=P_{\text{H}_2\text{O}}/P_0$, where P_0 is the reference pressure set to 1 bar. For each reaction, above the curve, the sorbent absorbs CO_2 and the reaction goes forward to form Li_2CO_3 , whereas below the curve, the carbonate releases CO_2 and the reaction goes backward to regenerate the sorbent.

Figure 8. $\text{Li}_2\text{CuO}_2\text{-CO}_2\text{-H}_2\text{O}$ thermogravimetric kinetic isotherms performed at different temperatures (40, 60 and 80 °C) and RH (20, 40, 60 and 80 %).

Figure 9. XRD pattern of the $\text{Li}_2\text{CuO}_2\text{-CO}_2\text{-H}_2\text{O}$ isothermal product treated at 80 °C with 80 % of RH.

Figure 10. TG and DTG decomposition curves of $\text{Li}_2\text{CuO}_2\text{-CO}_2\text{-H}_2\text{O}$ products treated isothermally at 80 °C and different RH (20-80 %).

Figure 11. Quantification of the CO_2 desorbed during the TG analyses from Li_2CO_3 by Li_2CuO_2 varying temperature and RH.

Figure 12. Secondary (A) and backscattered (B) electron images of the $\text{Li}_2\text{CuO}_2\text{-CO}_2\text{-H}_2\text{O}$ isothermal products treated at 80 °C with 80 % of RH.

Figure 13. N_2 adsorption-desorption isotherm of the pristine Li_2CuO_2 sample and the $\text{Li}_2\text{CuO}_2\text{-CO}_2\text{-H}_2\text{O}$ isothermal product treated at 80 °C and 80 % of RH.

TABLES

Table 1. The calculated thermodynamic properties of reaction of CO₂ captured by Li₂CuO₂ and LiOH comparison with Li₂O. T₁ and T₂ are the turnover temperatures of the CO₂ capture reactions at P_{CO₂} =0.1 bar for post-combustion, P_{CO₂}=20 bar for pre-combustion condition. For LiOH, assuming P_{H₂O}=1 bar.

Reactions	CO ₂ wt%	ΔE^{DFT} (kJ/mol)	ΔH (kJ/mol)	ΔG (kJ/mol)	T ₁ (K)	T ₂ (K)
Li ₂ CuO ₂ + CO ₂ = Li ₂ CO ₃ + CuO	59.99	-190.052	-184.516	-135.359	1005	1335
2LiOH + CO ₂ = Li ₂ CO ₃ + H ₂ O	91.88	-76.659	-98.623	-97.134	H _t ^a	H _t
Li ₂ CuO ₂ + H ₂ O = 2LiOH + CuO	---	-113.393	-85.893	-38.225	---	---
Li ₂ O + CO ₂ = Li ₂ CO ₃ ^b	142.52	-204.786	-226.731	-179.261	1295	H _t

^a H_t stands for the temperature out of the range of 1500 K

^b Taken from Refs 51 and 63.

Figure 1

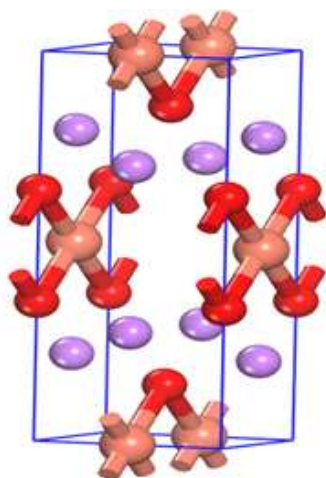


Figure 2

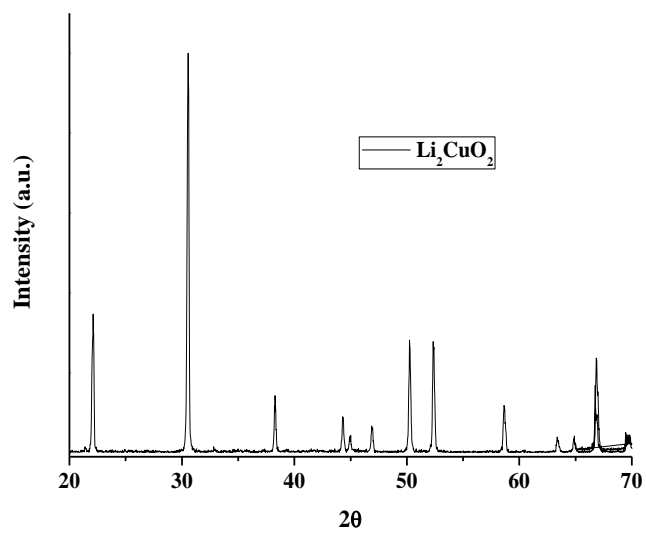


Figure 3

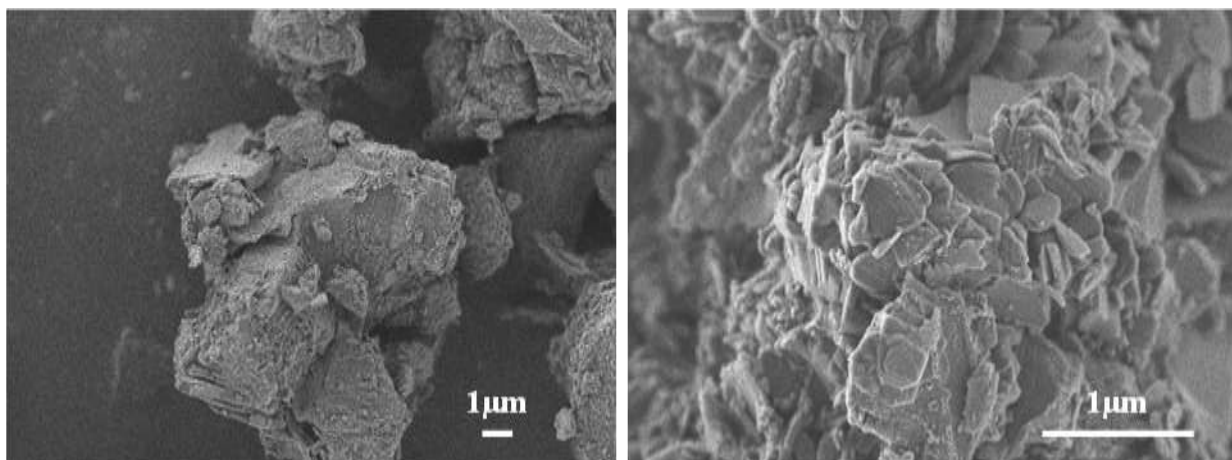


Figure 4

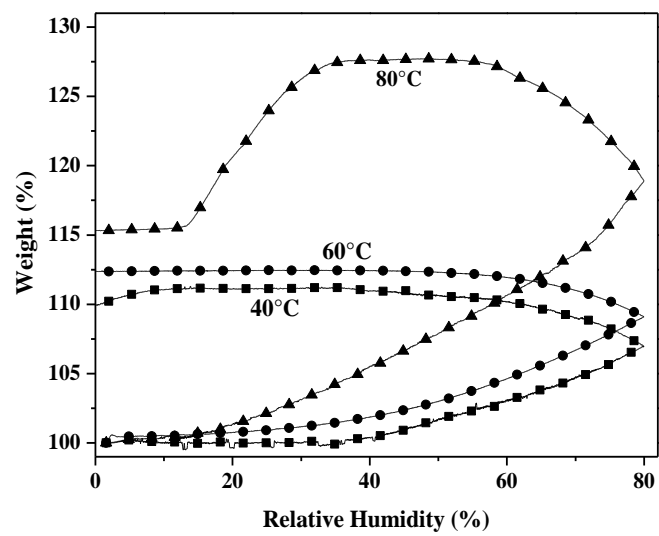


Figure 5

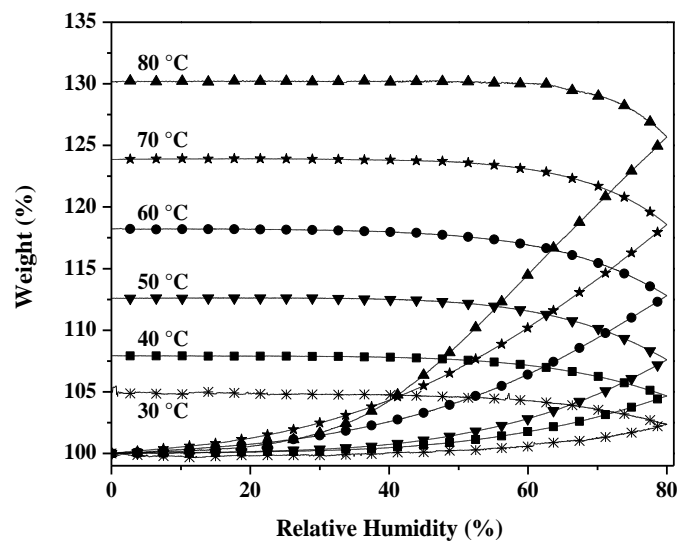


Figure 6

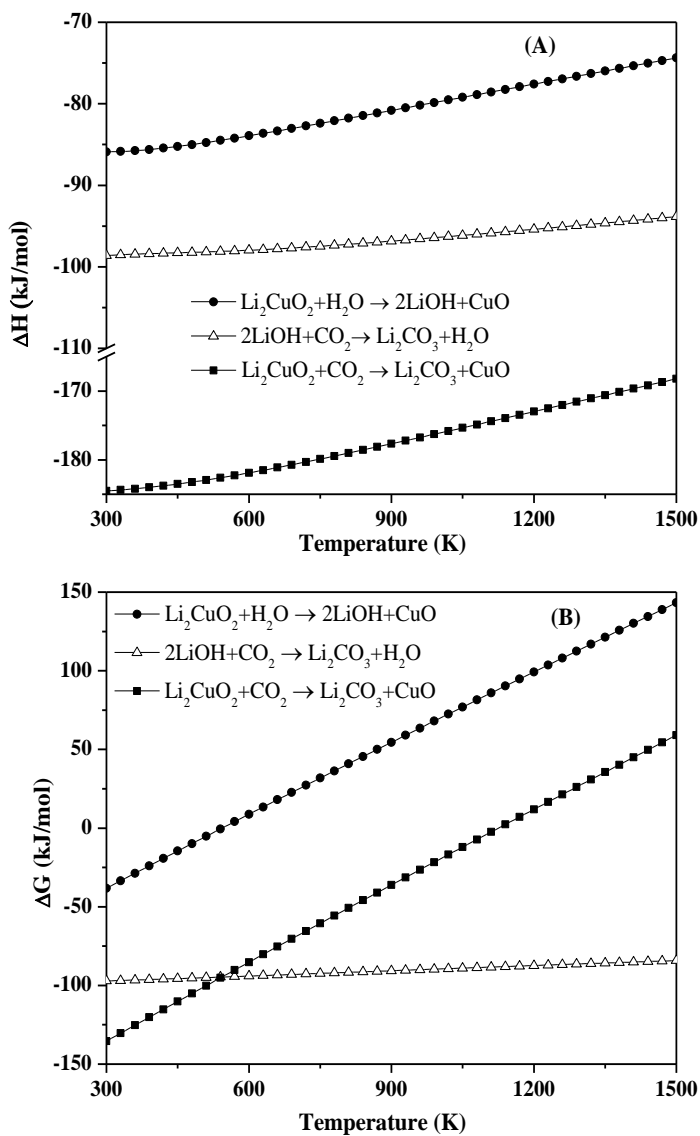


Figure 7

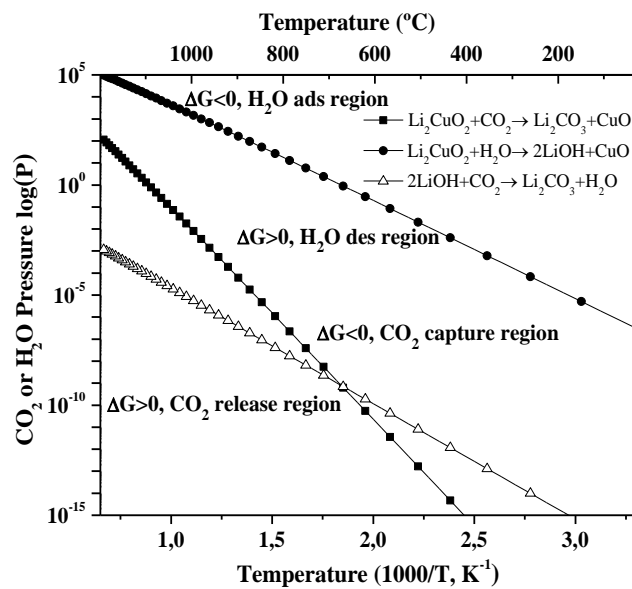


Figure 8

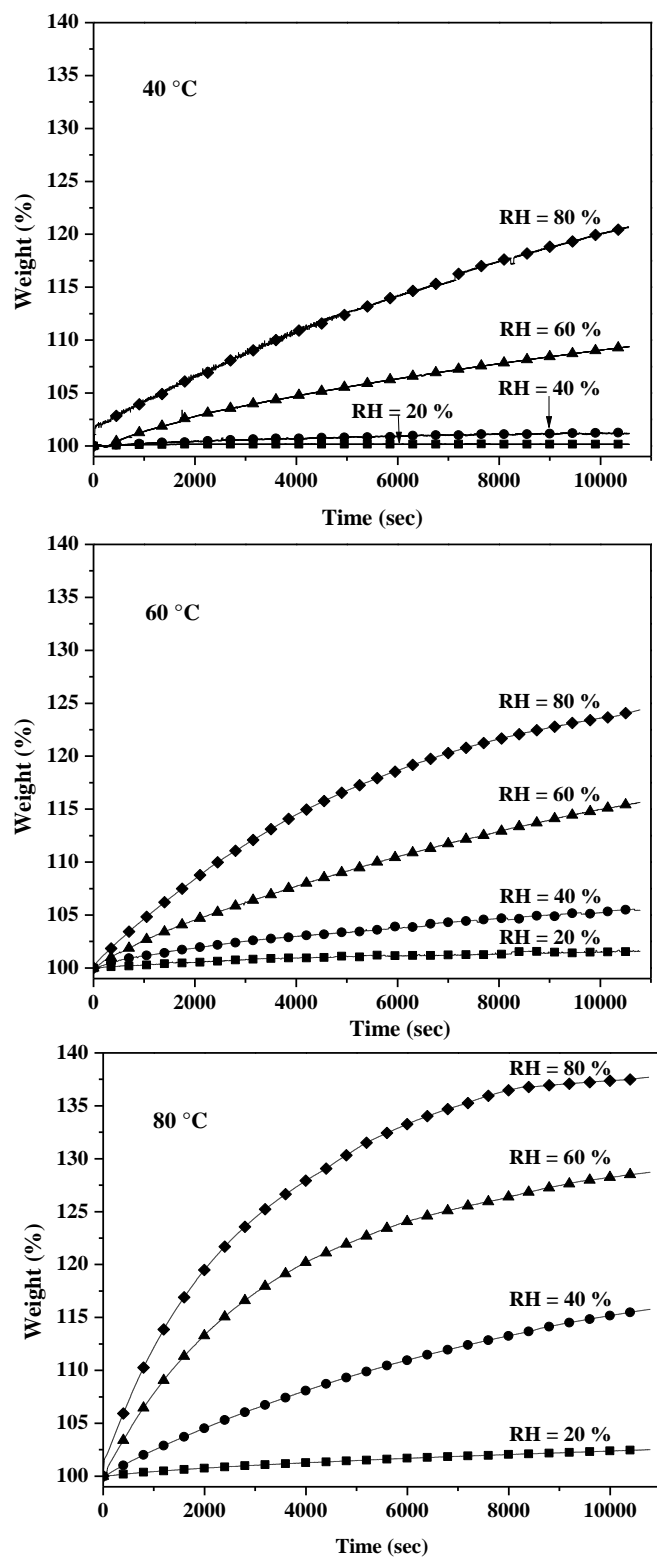


Figure 9

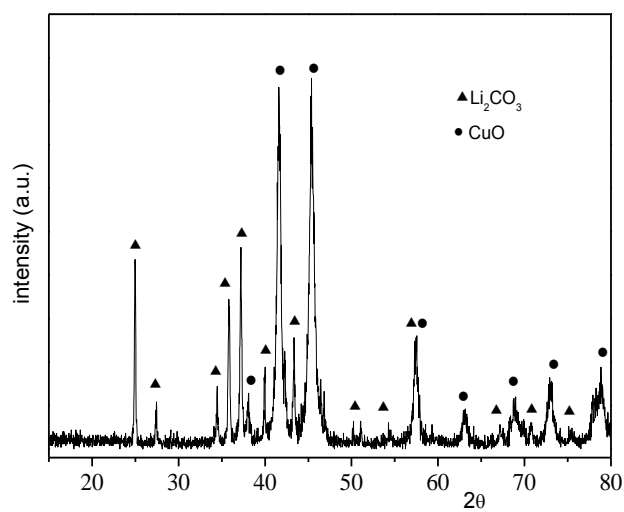


Figure 10

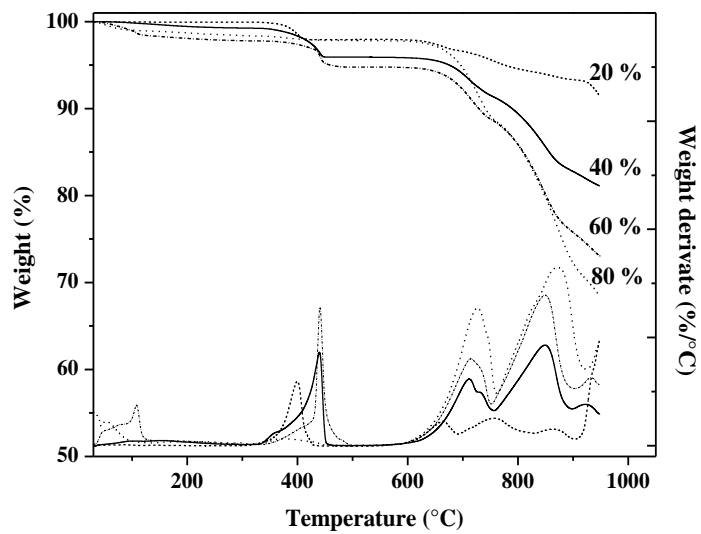


Figure 11

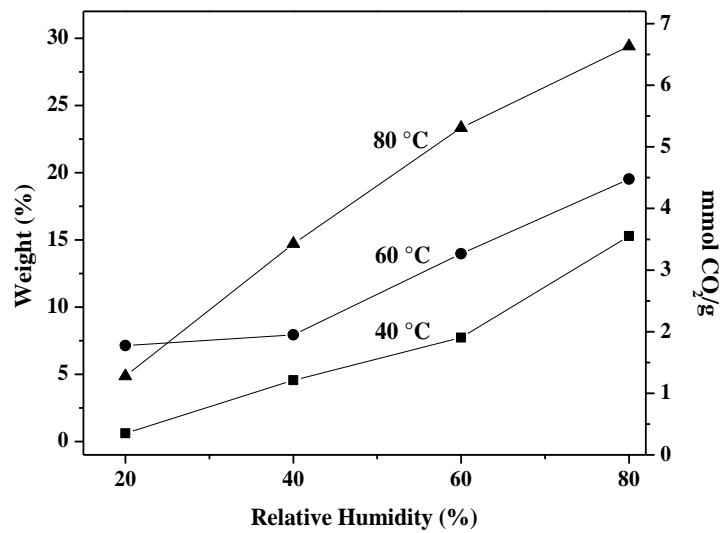


Figure 12

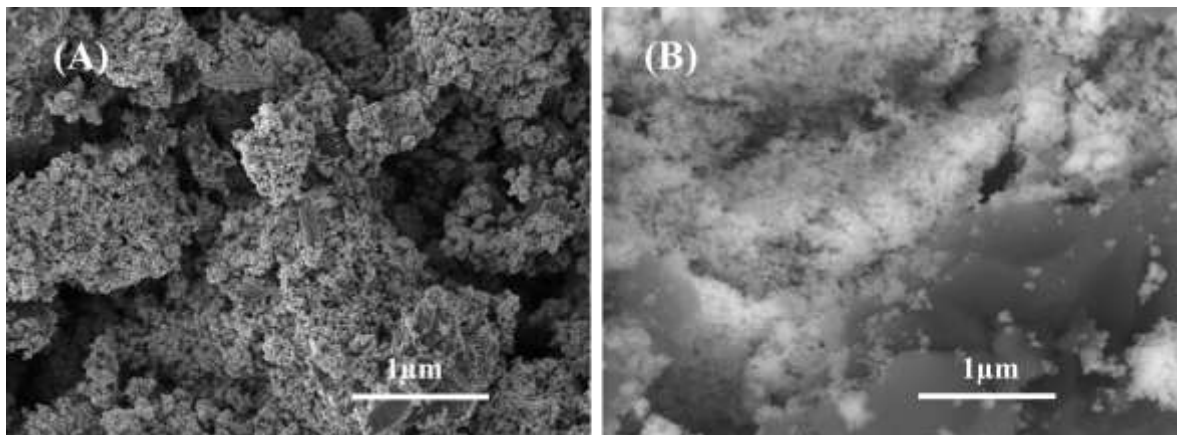


Figure 13

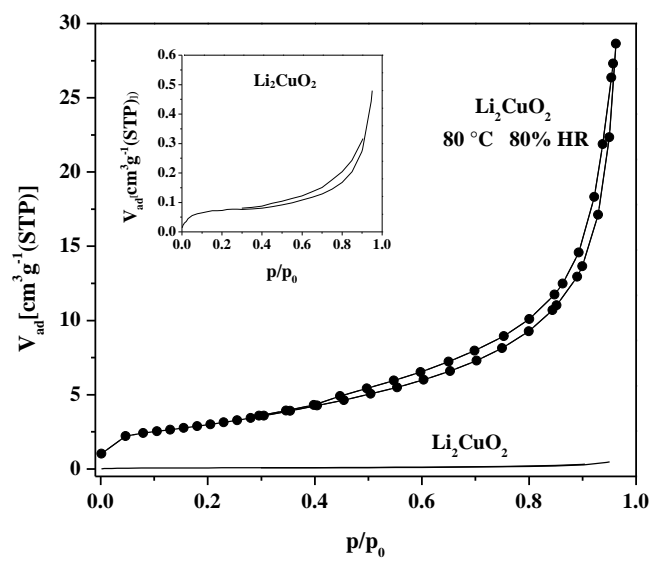
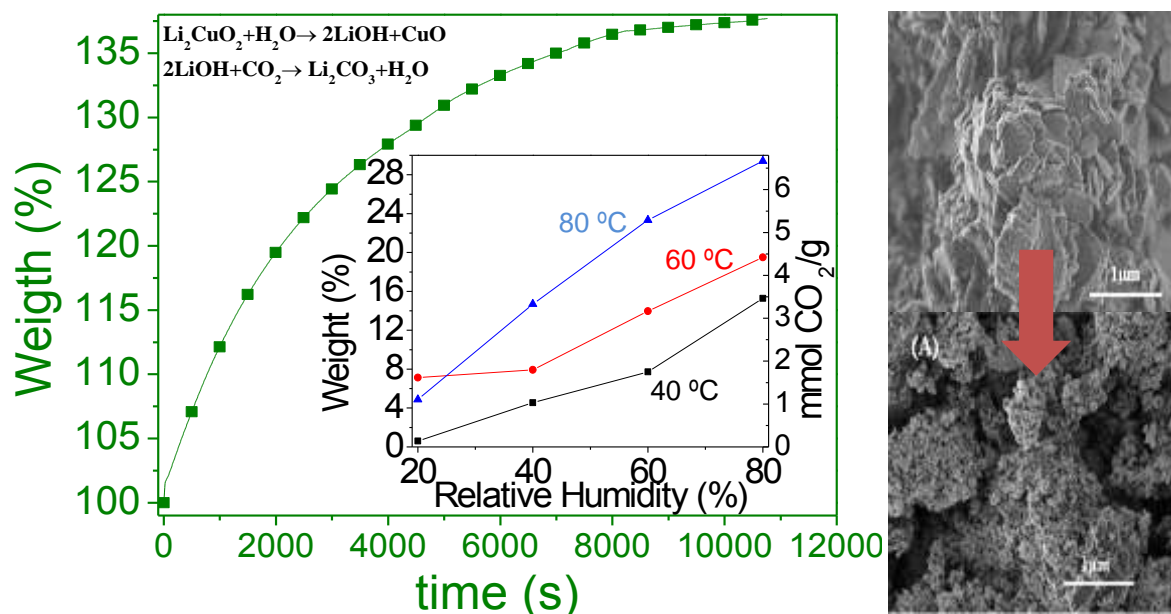


TABLE OF CONTENTS



Li_2CuO_2 is able to chemisorb high quantities of CO_2 in the presence of water steam at low temperatures